Pol. J. Environ. Stud. Vol. 32, No. 1 (2023), 943-951
DOI: *10.15244/pjoes/155201* ONLINE PUBLICATION DATE: 2022-12-23

Original Research

Study on Delaying Frost Growth Performance of Micro-Nanostructure Superhydrophobic Copper Surfaces

Siyu Zhao[1], Songyuan Zhang[2], Zhong Ge[1*], Jian Li[3], Jianbin Xie[1], Jian Xu[1], Zhiyong Xie[1], Kerun Yu[4]**

[1]School of Architecture and Urban Planning, Yunnan University, Kunming 650500, Yunnan, China
[2]Faculty of Metallurgical and Mining, Kunming Metallurgy College, Kunming 650033, China
[3]School of Mechanical Engineering, Beijing Institute of Technology, Beijing 100081, PR China
[4]School of Environmental Science and Technology, Dalian University of Technology, Dalian 116024, China

Received: 16 August 2022
Accepted: 6 October 2022

Abstract

In this work, the superhydrophobic surfaces with micro-nano composite structure was successfully prepared by one-step electrodeposition based on Ca-myristic acid complex onto Cu substrate. The performance of delaying frost growth on micro-nanostructure superhydrophobic copper surfaces was explored, and the application of superhydrophobic materials in organic rankine cycle (ORC) was simulated. The experimental results confirmed that the superhydrophobic surfaces increased the nucleation barrier of the condensation droplets, enhanced the heat transfer resistance between the condensation droplets and the cold surface, and effectively restrained frost growth. The simulation study of superhydrophobic materials in organic rankine cycle (SH-ORC) system and ORC system was carried out with Matlab software. It was proved that the net power output and exergic efficiency of SH-ORC system were significantly increased compared with that of ORC system. When the heat source temperature was 180ºC, the net output power of SH-ORC was 15.07% higher than that of ORC, and the exergy efficiency was greater than 14%. The simulation results showed that the most suitable heat source temperature for SH-ORC was 180ºC. Therefore, the superhydrophobic copper surfaces can be potentially used to minimize frost formation in harsh environment.

Keywords: superhydrophobic surfaces, micro-nano structure, delaying frost growth, numerical simulation

*e-mail: ynuzhongge@163.com
**e-mail: thulijian@163.com

Introduction

After more than 40 years of rapid development in economic field, China's energy demand has been continually increasing in recent years [1]. It is estimated that building energy consumption accounts for 22% of the total annual energy consumption in 2019 [2]. In some areas with low temperature and high humidity in winter, large-scale heating has not yet been realized. When residents use air conditioning for heating in winter, the harsh environment will lead to frost of outdoor air conditioning units, thus reducing the efficiency of air conditioning. Previous studies showed that the overall efficiency of heat exchanger decreased by 50% to 75% with the increase of running time [3]. Recent research results confirmed that the superhydrophobic surface (water contact angle is greater than 150°) had the functions of enhancing heat transfer, frost suppression, self-cleaning and corrosion resistance [4-8].

Many scholars have made a lot of research results on how the superhydrophobic surface plays a role in delaying frost growth. Ji et al. [9] calculated the pore deformation ratio of the PVDF (polyvinylidene) membrane reinforced by PDMS (polydimethylsiloxane) (PVDF@PDMS) and the pristine PVDF fiber membrane by the ABAQUS software. The pore deformation ratio of the PVDF membrane reinforced by PDMS (PVDF@PDMS) (pore deformation ratio is 0.036) was hundreds of times smaller than the pristine PVDF fiber membrane (pore deformation ratio is 7.685). Wang et al. [10] simulated stress distribution on the inverted-pyramidal microstructures and the microstructure framework consisted of an array of microscale inverted-pyramidal cavities. It is proved that the microstructure has good mechanical durability. The surfaces maintained a static contact angle of greater than 150º and a roll-off angle of less than 12º after 1000 abrasion cycles. Researchers used this strategy to create a robust and self-cleaning topcoat for solar cells. This topcoat enabled high energy-conversion efficiency to be maintained through the passively removing of dust contamination, which could lead to large savings in terms of freshwater, labour and cost compared with the traditional cleaning process. Li et al. [11] prepared a superhydrophobic smart coating for flexible and wearable sensing electronics, which showed superior sensitivity (gauge factor of 5.4-80), high resolution (1º of bending), a fast response time (<8 ms), a stable response over 5000 stretching-relaxing cycles, and wide sensing ranges (stretching: over 76%, bending: 0-140º, torsion: 0-350 rad m^{-1}). Chen et al. [12] fabricated the hydrophobic microgripper which employed inertia force to overcome adhesion force achieving. Dhillon et al. [13] enhanced the critical heat flux (CHF) of industrial boilers by surface texturing, which could effectively facilitate boiling. This technique is used in the evaporator of ORC system [14]. Experimental results show that the superhydrophobic outdoor condenser under frosting condition has a higher energy conversion rate (more than 85%) than the traditional hydrophilic condenser [15]. Chen [16] et al. designed a multi-scale pyramid conical nanostructure surface with both hydrophilic and superhydrophobic, on which droplets were easily condensed and self-bounce cleared with good hydrobicity. Ashiqur et al. [17] investigated the effect of microgroove geometry on frosting and meltwater drainage on aluminum and copper surfaces. Some researchers have made a detailed theoretical explanation and experimental proof of heat exchange and heat transfer properties on superhydrophobic surface, as well as the influence of the surface microstructure [18-19]. The preparation and delaying frost growth performance of superhydrophobic surface materials were discussed in the above literature, and the specific microscopic process of frost formation and restraining the frost growth on superhydrophobic surface were observed and studied. However, there are few observation and analysis of edge frost on metal surface, and there is no literature on the application of superhydrophobic materials in ORC.

In this paper, one-step electrochemical deposition method [6] was used to prepare superhydrophobic coating with micro-nano composite structure on copper surfaces. The frosting experiment was carried out through a low temperature thermostat, and the frost edges of different copper sheets were visualized by using a forward metallographic microscope. The surface morphology and chemical composition of the coating samples were characterized using scanning electron microscopy (SEM, JEOL, JSM-7500F) and energy-dispersive spectroscopy (EDS). The water contact angles were measured (CHD-JCJ180A-1, Dongguan Chengding Instrument Technology Co., LTD) at the ambient temperature. At the same time, relevant theories were used to explain the experimental phenomena. The effect of superhydrophobic surfaces on the net power output of ORC system was simulated by Matlab.

Experimental

Preparation of the Samples

During the research, copper plate (20 mm×20 mm ×1 mm, 99.9 % of purity, Guantai Metal Materials Co., LTD., Hebei Province) was used as the substrate for electrodeposition process. All reagents used in this experiment were of analytical grade and were used without further purification. Before experiments, the copper substrates were polished with metallographic sandpaper from 1000 grid to 1500 grid and cleaned with anhydrous alcohol and acetone in an ultrasonic cleaner for 3 min. Two copper plates worked as both cathode and anode with a direct current (DC) as the energy source (CSYJ12-500, Dongguan Koshiyuan Electronic Technology Co., LTD., Guangdong Province). The distance between the two electrodes was 2 cm

to ensure that there was no short circuit to occur. The electrolyte volume was 100 mL ethanol solution containing 0.82g calcium chloride and 1.83g myristic acid. The electrolyte was initially stirred with a glass rod and then ultrasonic for 30 min to obtain a uniform solution for electroplating experiment. The electrodeposition reaction was performed at room temperature with a DC voltage of 27.5V and an electrolytic time of 30 min. When the deposition process was completed, the cathode copper plate was brought out and the copper sheet covered by the sediment was washed several times with deionized water and ethanol, respectively. Then the prepared samples were dried at room temperature and stored in a desiccator for subsequent experiments.

Frost Experiments

The samples were placed on a low temperature thermostat (DC-2006+KXN-305D, Jiangsu Tianying Instrument Co., LTD) and the experiment of frost growth was carried out under strictly controlled values of the operating parameters. The characteristics of frost formation and growth on the surface of copper samples were investigated under the natural convection condition, the temperature of low temperature thermostat was -20ºC, the air temperature was 18ºC and the relative humidity was 68%. Condensation and frost formation processes were also examined under a metallographic microscope (TXL-3230BD, Shanghai Research Instrument Co., LTD) on a set of copper surfaces.

Results and Discussion

Water Contact Angle and SEM

Taking a contact angle meter as the platform, the surface wettability was measured with water droplet having volume of 3 μL at room temperature. The deposition time of droplets on the surfaces is very short, so the effect of droplet evaporation can be ignored during contact angle measurement. After continuous electrodeposition at a constant voltage of 27.5V for 30 min, the maximum value of water contact angle (WCA) on the electrodeposited copper surfaces was measured to be 152.06° (Fig. 1a).

The microscopic surface morphology of cathode copper after electrodeposition is shown in Fig. 1. The surface of electrodeposited cathode copper sheets has spherical micron structure, while the surface has irregular strip nanostructures at different magnifications (Fig. 1b and c). It can be seen that micro-nano structure is formed on the surface of electroplated cathode copper surfaces. The EDS result of cathodic copper after electroplating (Fig. 1d) affirmed the existence of C, O and Ca elements in the superhydrophobic copper sheets, and the content of carbon, oxygen and calcium is 77.03%, 17.09% and 9.73%, respectively.

ORC Model

The superhydrophobic surface of micro/nano composite structure can increase nucleation cavity, which is beneficial to the phase transformation heat

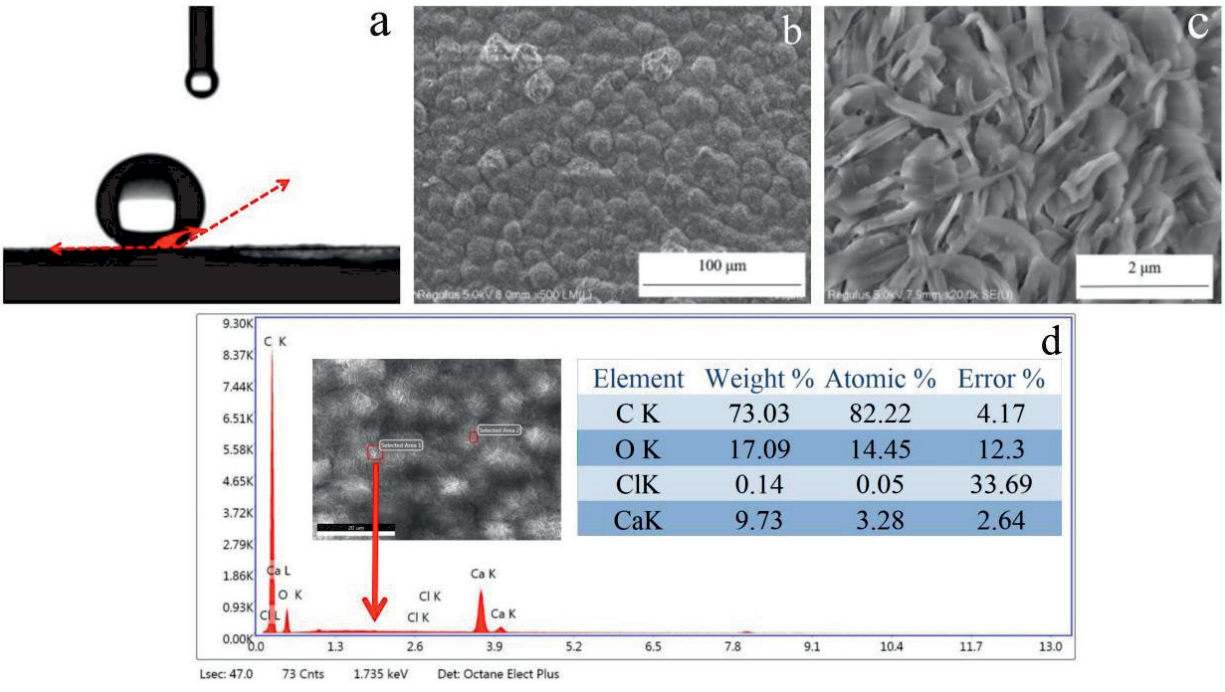

Fig. 1. a) WCA of cathodic copper surfaces after electroplating. SEM images of cathodic copper surfaces after electroplating (b and c); (d) EDS of cathodic copper surfaces after electroplating.

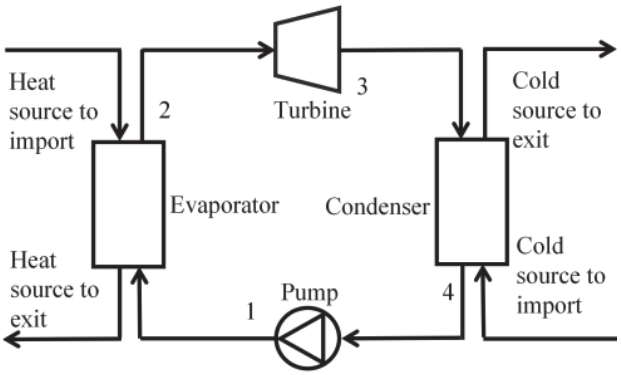

Fig. 2. Schematic diagram of ORC system.

of working medium. The research results of Liu et al. showed that the average heat transfer coefficient of superhydrophobic micro-nano composite structure was 16.1% higher than that of ordinary surface [14]. The net output power can be increased and the exergy loss can be reduced if the superhydrophobic micro-nano composite structure material is used in the ORC evaporator. The ORC system was constructed by Matlab2017a to simulate its thermodynamic performance, and the physical parameters used were all from REFPROP9.0. The circulation diagram of ORC is presented in Fig. 2. The working medium used for this numerical simulation is all R123 [20]. Table 1 lists the boundary conditions of the system model.

The used assumptions are shown as follows:

1) The hot fluid and organic working medium are in a steady flow state during each cycle stage.

2) The isentropic efficiency of organic working fluid in working medium pump and turbine does not change with the change of working condition.

3) Heat loss is negligible in heat exchangers and pipes.

Table 1. Parameter settings of ORC system.

Parameter	Numerical value
Temperature of the heat source/ºC	120~200
Thermal fluid flow rate/(kg·s^{-1})	1
Thermofluid pressure/Mpa	1.6
Transequal entropy efficiency/%	0.8
Isentropic efficiency of working medium pump/%	0.75
Cooling water inlet temperature/ºC	25
Cooling water temperature rise/ºC	5
Evaporator pinch point temperature difference/ºC	3~27
Temperature difference between condenser clamp point/ºC	5
Environment temperature/ºC	20

4) The effects of gravitational potential energy and kinetic energy of organic working fluid in the inlet and outlet of pump are ignored.

System Model Equations

The heat absorption capacity of the ORC system is [21-25]

$$Q_{\text{sys}} = m_{\text{HS}}(h_{\text{HS,in}} - h_{\text{HS,out}}) \tag{1}$$

where $h_{\text{HS,out}}$ and $h_{\text{HS,in}}$ are heat source fluid enthalpies at the system outlet and inlet, respectively.

The mass flow rate of working fluid is determined by:

$$m_{\text{f}} = Q_{\text{sys}}/(h_2 - h_1) \tag{2}$$

The cooling water mass flow rate is

$$m_{\text{cool}} = \frac{m_{\text{f}}(h_3 - h_4)}{h_{\text{cool,out}} - h_{\text{cool,in}}} \tag{3}$$

The power output generated by the turbine is

$$W_{\text{Tur}} = m_{\text{f}}(h_2 - h_3) \tag{4}$$

The power consumed by the working fluid pump is

$$W_{\text{Pump}} = m_{\text{f}}(h_1 - h_4) \tag{5}$$

The net power output of the ORC system can be determined by a formula

$$W_{\text{net}} = W_{\text{Tur}} - W_{\text{Pump}} \tag{6}$$

The efficiency of the second law of thermodynamics is calculated as

$$\eta_{\text{ex}} = \frac{W_{\text{net}}}{E_{\text{ex,in}}} \tag{7}$$

$$E_{\text{ex,in}} = m_{\text{HS}}[(h_{\text{HS,in}} - h_0) - T_0(s_{\text{HS,in}} - s_0)] \tag{8}$$

Exergy destruction (E_H) is given as

$$E_{\text{H}} = m_{\text{HS}}[(h_{\text{HS,in}} - h_{\text{HS,out}}) - T_0(s_{\text{HS,in}} - s_{\text{HS,out}})] - m_{\text{f}}[(h_2 - h_1) - T_0(s_2 - s_1)] \tag{9}$$

Exergy destruction of heat rejection ($E_{HS,out}$) is calculated as

$$E_{\text{HS,out}} = m_{\text{HS}}[(h_{\text{HS,out}} - h_0) - T_0(s_{\text{HS,out}} - s_0)] \tag{10}$$

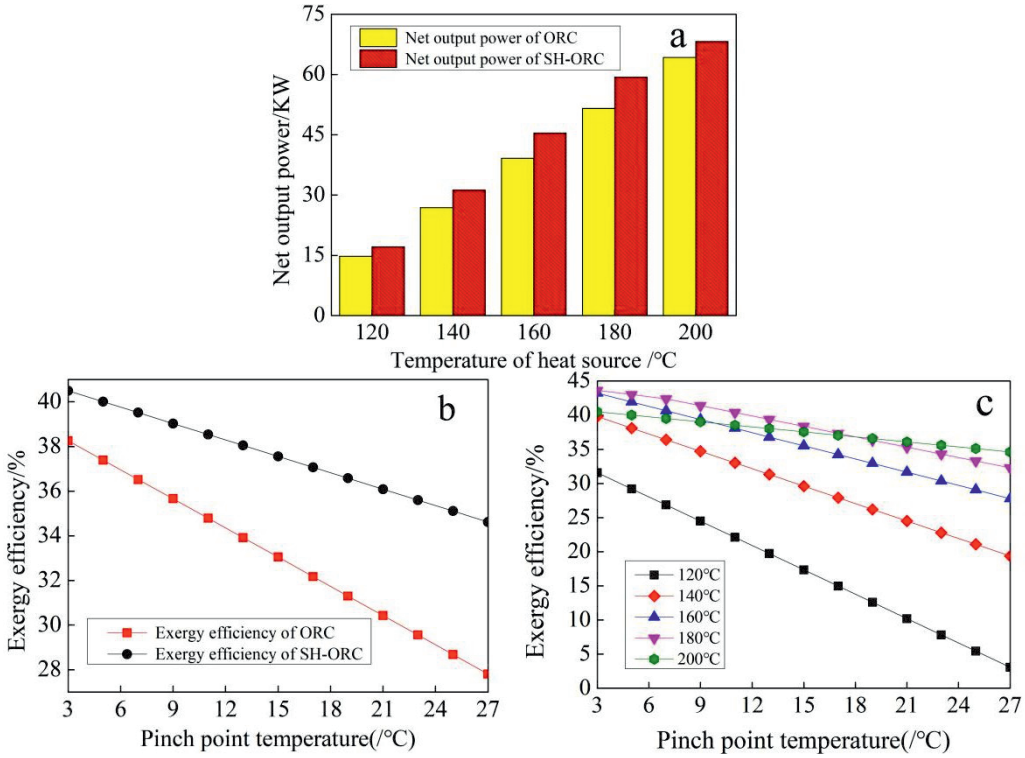

Fig. 3. Net output power of SH-ORC and ORC at different heat source temperatures (a); Exergy efficiency of SH-ORC and ORC at different differences of pinch point temperature (b); Exergy efficiency of SH-ORC variation with temperature difference of pinch point under different heat source temperature (c).

Exergy destruction of the turbine (E_{Tur}) is

$$E_{\mathrm{Tur}} = m_{\mathrm{f}} - T_0(s_3 - s_2) \tag{11}$$

Exergy destruction of condensator (E_{cold}) can be determined by a formula

$$E_{\mathrm{cold}} = m_{\mathrm{f}}[(h_3 - h_4) - T_0(s_3 - s_4)] \tag{12}$$

Exergy destruction of working medium pump (E_{pump}) can be obtained

$$E_{\mathrm{Pump}} = m_{\mathrm{f}} T_0(s_1 - s_4) \tag{13}$$

E_{tot} is the total exergy and is defined as

$$E_{\mathrm{tot}} = E_{\mathrm{H}} + E_{\mathrm{HE,out}} + E_{\mathrm{Tur}} + E_{\mathrm{cold}} + E_{\mathrm{Pump}} \tag{14}$$

Under different heat source temperatures, the net output power of SH-ORC and ORC is shown in Fig. 3a). The net power output of SH-ORC is more than 16% higher than that of ORC in the range of 100-160ºC. When the heat source temperature is 180ºC, the increase ratio of net output power is 15.07%. However, when the temperature is 200ºC, the increase rate of net output power is significantly reduced to 6.24%. Therefore, compared with ORC, SH-ORC is more suitable for collecting low temperature waste heat below 180ºC. As shown in Fig. 3b), exergic efficiency of both SH-ORC and ORC decreased with the increase of the temperature difference of the evaporator pinch point, but exergic efficiency of SH-ORC was always higher than that of ORC, and the exergic efficiency of SH-ORC decreased at a lower rate than that of ORC. Meanwhile, exergic efficiency of SH-ORC was always 14% higher than that of ORC under the simulated conditions, and the maximum value can reach 16.1%.

Based on the above analysis, the performance of SH-ORC is better than that of ORC. Fig. 3c) shows the variation of the exergic efficiency of SH-ORC with the temperature difference at the pinch point under different heat source temperatures. At the same heat source temperature, exergic efficiency decreased with the increase of temperature difference of evaporator pinch point. With the increase of heat source temperature, exergic efficiency of the system first increased and then decreased. When the temperature difference of pinch point is less than 18ºC, the heat source temperature of 180ºC is the most suitable for exergic efficiency of the system. As the temperature difference is greater than 18ºC, the heat source temperature of 200ºC is the best fit for the exergy efficiency of the system. It can be seen from Fig. 3 that the heat source temperature of 180ºC is the most suitable for SH-ORC system when the temperature difference of pinch point is less than 18ºC.

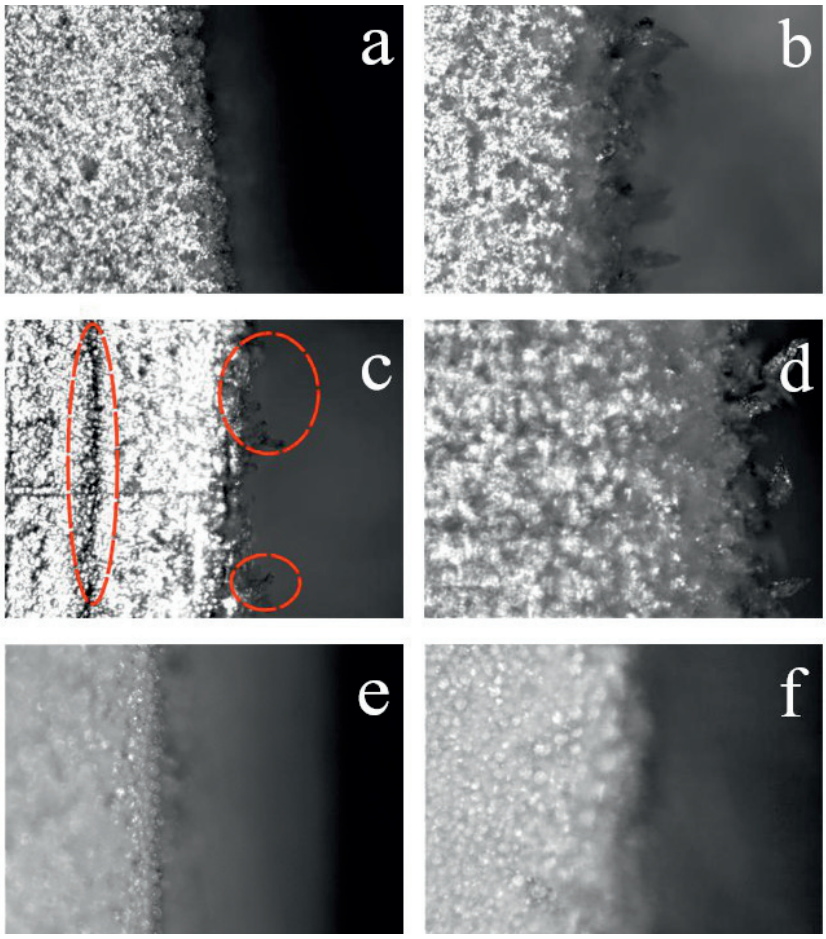

Fig. 4. Comparison of frost on copper surfaces at -20ºC (Polished the surface for 10 min (a) and 30min (b); Unpolished the surface for 15 min (c) and 30min (d); Electrodeposited surface 30min (e) and 40min (f)).

Analysis of Frosting

In order to see clearly the frost phenomenon, all the photos taken in this paper are the right edge of the copper at 100 times magnification. The analysis of the red circles in Fig. 4c) shows that the condensation droplets on the metal surface mainly come from edges or structural defects. As shown in Fig. 4a), when the experiment of frost formation was carried out for 10 min, frost crystals with small size and regular shape appeared on the surface edge of the polished copper sheet and diffused from the edge to the center. When the experiment of frost formation was carried out for 15 min, irregular frost layer began to appear on the edge of the unpolished copper sheet (Fig. 4c). Frost crystals have not formed completely on the surface of the copper sheet, while frost crystals in some areas have started to generate the irregular shape of the branches grow outward. The condensation droplets are more dense on structural defects in comparison to smooth surface. When the experiment was carried out for 30 min, there were only condensation droplets which had not been completely frozen at the edge of the electroplated copper sheet, and the complete frost crystal had not been formed at this time. The experiment of frosting time was carried out for 30 min, at this time, the frost layer on the surface of the polished copper sheet (Fig. 4b) and the unpolished copper sheet (Fig. 4d) had obvious thickness, and a large number of dendritic frost crystals were produced on the outermost surface of the frost layer. The surface is almost completely covered by frost crystals. The droplets on the electroplated copper sheet have not been completely frozen at 30 min of the experiment (Fig. 4e), while at the edge of the electroplated copper sheet has formed obvious frost layer at 40 min of the experiment (Fig. 4f). Previous studies have also reached similar conclusions on the sequence of initial frosting time of polished copper sheet, unpolished copper sheet and electroplated copper sheet [26]. In summary, the condensation phase and the droplet freezing phase on the surface of the electroplated copper sheet will last for a long time, so the surface of the electroplated copper sheet can effectively delay frosting.

According to the analysis in Fig. 4, the frosting first starts at the edge of metal surface and structural defects, and then spreads to the central surface. Chen et al. [27] also reported similar phenomena in their previous paper. On the metal surface, the latent heat of liquid-solid phase transition is completed by conducting

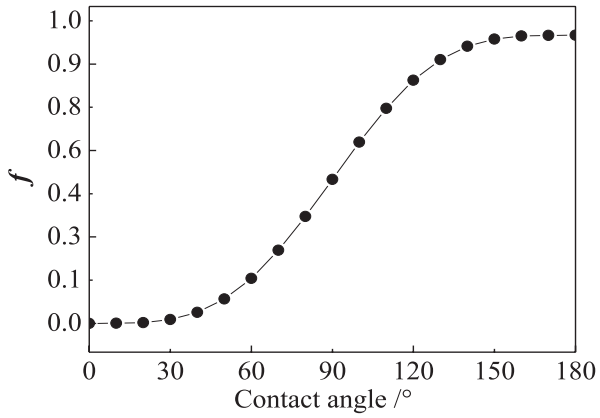

Fig. 5. Effect of WCA on nucleation barrier.

heat on the cold surface. Compared with the droplets on the ordinary surface, the contact area between the droplets and the superhydrophobic surface is relatively small when the droplet volume is the same, which reduces the heat transfer rate of the latent heat of liquid-solid phase transition.

Because the contact area is small, the height of the droplet in the vertical direction is relatively high, which will increase the heat transfer resistance of the frost crystal. From the analysis of Equations 15 and 16, it can be seen that the thermal resistance of heat conduction inside the droplet and the cold surface also increase significantly with the increase of contact angle. In conclusion, the effect of frost suppression on superhydrophobic surface is particularly excellent from the time of droplet generation to frost formation.

The thermal resistance of heat conduction inside the droplet (R_{drop}) and the thermal resistance of heat conduction on the cold surface (R_W) [28, 29] is determined

$$R_{\text{drop}} = \frac{\theta}{2k_{\text{in}}\pi\sin\theta} \tag{15}$$

$$R_{\text{W}} = \frac{A_{\text{W}}}{k_{\text{W}}\pi r_{\text{s}}^2\sin^2\theta} \tag{16}$$

Where θ is contact angle, and A_W is area of base. A_{drop} is the area of contact between saturated wet air and the surface of the droplet. k_{in} and k_W are the thermal conductivity of the droplet and cold surface, respectively.

It is observed that the surface of the copper is dominated by cold condensation frost at -20ºC [30]. Only when the change of free energy of water vapor on the surface of copper sheet exceeds the critical nucleation barrier (ΔG) can it condense successfully. The nucleation barrier (ΔG) mainly consists of two parts, namely, the change of volume free energy for condensation of saturated vapor into droplets and the free energy required for formation of droplets on the surface. When water vapor condenses on a cold surface, the change in Gibbs free energy energy and barrier coefficient (f) can be calculated by the following equation [30, 31].

$$\Delta G = \frac{4\pi M^2\gamma_{lg}^3}{3(R\rho_1 T_{\text{W}}\ln\frac{P_{\text{v}}}{P_{\text{s}}})^2}(2-3\cos\theta+\cos^3\theta) \tag{17}$$

$$f = \frac{2-3\cos\theta+\cos^3\theta}{4} \tag{18}$$

Fig. 5 reveals the relationship between energy barrier coefficient (f) and contact angle when other conditions are assumed constant. It can be seen from Fig. 5 that the energy barrier coefficient increases with the increase of contact angle. It is therefore more difficult for water vapor to condense into droplets on a superhydrophobic surface than on a normal surface. In conclusion, the superhydrophobic copper surfaces has a good effect on delay frost formation in the early frosting stage.

Conclusions

A superhydrophobic coating with micro/nano structure was prepared on copper surface by one-step electrochemical deposition. The maximum surface contact angle was measured to be 152.06°. The frosting experiment was carried out in a low temperature constant temperature tank, and the frosting phenomenon was observed and analyzed by metallographic microscope. At the same time, Matlab was used to simulate SH-ORC system and ORC system, and the improvement of ORC system performance by superhydrophobic materials was analyzed from the aspect of enhancing heat transfer coefficient. The following conclusions can be drawn:

(1) The superhydrophobic copper surfaces can effectively delay the formation of condensation droplets because of the larger contact angle and the larger nucleation barrier. Compared with the other two copper pieces after the same experiment for 30 min, the effect of frost suppression is obvious.

(2) The surface of the superhydrophobic material has micro/nano structure, and the number of nucleated holes is increased when the working medium is transformed from liquid to gas, so as to improve the average heat transfer coefficient. Compared with the ORC system, the net output power and exergy efficiency of SH-ORC were significantly improved. The simulation results show that the heat source temperature of 180ºC is the most suitable for SH-ORC.

Future Work

It has been reported that the superhydrophobic surfaces can enhance the heat transfer resistance [32],

and its application in evaporator can improve the overall performance of the system [14]. In addition, it has also been reported that the application of superhydrophobic coating on air conditioning system can effectively delay the growth of frost [33]. Superhydrophobic coatings can also be used in other industrial areas affected by frost formation. Analysis of factors affecting frost of superhydrophobic coating is helpful to understand the frost formation mechanics and anti-frost methods. However, the selections are limited by the availabilities of precise thermo-physical properties and heat transfer correlations at present. The mechanisms are still not well understood and need further study.

Acknowledgments

It is gratefully acknowledged that this work is supported by Research Fund of Yunnan Province (Grant No.202001BB050070), the National Natural Science Foundation of China (Grant Nos.52106017,51878591,11862024), Yunnan Provincial Department of Education Science Research Fund Project (Grant No.2019J0025), Talent Project of Yunnan University (Grant No.C176220200), Scientific Research Foundation of Kunming Metallurgy College (Grant No.Xxrcxm201802), Beijing Natural Science Foundation (Grant No.3222031), the Postgraduate Research and Innovation Foundation of Yunnan University (Grant No.2021Y284).

Conflict of Interest

The authors declare no conflict of interest.

References

1. LIU A.H., YE Z.C. China Statistical Yearbook 2020. Beijing: China Statistics Press, **2021**.
2. JIANG Y. China building energy consumption annual report 2020. Journal of BEE. **49** (02), 1, **2021**.
3. CUI J., LI W.Z., LIU Y., Zhao Y.S. A new model for predicting performance of fin-and-tube heat exchanger under frost condition. Int. J. Heat. Fluid. Fl. **32** (1), 249, **2010**.
4. CHEN X.M., JUSTIN A., WEIBEL, SURESH V., GARIMELLA. Exploiting microscale roughness on hierarchical superhydrophobic copper surfaces for enhanced dropwise condensation. Adv. Mater. Interfaces **2** (3), 1400480, **2015**.
5. CHEN J.Y., CHEN J.W., LI L., WANG S.W., XIE Y. Study on the self cleaning phenomenon and anti-pollution flash over performance of micro-nanostructure superhydrophobic coating surface under a high humidity environment. Colloid. Surface. A **630**, 127552, **2021**.
6. LI B.Z., ROBERT H.B. MILLER, ZHANG H.B., OU Y.Y.B., QIU R., HU S.G., NIU H.L. A facile one-step route to fabricate bio-inspired superhydrophobic matrix with high corrosion inhibition to Cu metal. Surf. Interfaces **25**, 101189, **2021**.
7. LI B.Z., OU Y.Y.B., HAIDER Z.S., ZHU Y.H., QIU R., HU S.G., NIU H.L., ZHANG Y., CHEN M. One-step electrochemical deposition leading to superhydrophobic matrix for inhibiting abiotic and microbiologically influenced corrosion of Cu in seawater environment. Colloid. Surface. A **616**, 126337, **2021**.
8. JONATHAN B. BOREYKO C. PATRICK C. Delayed frost growth on jumping-drop superhydrophobic surfaces. ACS Nano. **7** (2), 1618, **2013**.
9. JI C.H., ZHU Z.G., ZHONG L.L., ZHANG W.M., WANG W. Design of firm-pore superhydrophobic fibrous membrane for advancing the durability of membrane distillation. Desalination **519**, 115185, **2022**.
10. WANG D.H., SUN Q.Q., MATTI J.H, ZHANG C.L., LIN F.Y., LIU Q., ZHU S.P., ZHOU T,F., CHANG Q., HE B., ZHOU Q., CHEN L.Q., WANG Z.K., ROBIN H.A.R., DENG X. Design of robust superhydrophobic surfaces. Nature **582**, 55, **2020**.
11. LI L.H., BAI Y.Y., Li L.L., WANG S.Q., ZHANG T. A superhydrophobic smart coating for flexible and wearable sensing electronics. Adv. Mater. **29**, 1702517, **2017**.
12. CHEN T., PAN M.Q., WANG Y.J., LIU J.Z., CHEN L.G., SUN L.N. Manipulation of microobjects based on dynamic adhesion control. Int. J. Adv. Robot. Syst. **9**, 89, **2012**.
13. NAVDEEP S.D., JACOPO B., KRIPA K.V. Critical heat flflux maxima during boiling crisis on textured surfaces. Nat. Commun. **6**, 8247, **2015**.
14. LIU G.L. Experimental study and optimization of organic rankine cycle power generation system and evaporator. Beijing: North China Electric Power University. **2021**.
15. WANG S.L., YUA X.Q., LIANG C.H., ZHANG Y.F. Enhanced condensation heat transfer in air-conditioner heat exchanger using superhydrophobic foils. Appl. Therm. Eng. **137**, 758, **2018**.
16. CHEN X.M., WU J., MA R.Y., HUA M., NIKHIL K., YAO S.H., WANG Z.K. Nanograssed micropyramidal architectures for continuous dropwise condensation. Adv. Funct. Mater. **21** (24), 4617, **2011**.
17. MD A.R., ANTHONY M.J. Experimental study on frosting/defrosting characteristics of microgrooved metal surfaces. Int. J. Refrig. **50**, 44, **2015**.
18. RYAN E., NENAD M., AHMED A.O., CARL V. THOMPSON, WANG E.N. Condensation on superhydrophobic surfaces: the role of local energy barriers and structure length scale. Langmuir **28** (40), 14424, **2012**.
19. NENAD M., RYAN E., WANG E.N. Effect of droplet morphology on growth dynamics and heat transfer during condensation on superhydrophobic nanostructured surfaces. ACS Nano. **6** (2), 1776, **2012**.
20. LIU J., WANG H.T., ZHANG S.Y., GE Z. Thermal performance comparative study of R123 and R245fa for organic rankine cycle. Renew. Energ. Resour. **34** (01), 112, **2016**.
21. HUANG G.D., ZHANG S.Y., Ge Z., XIE Z.Y., XIANG H.J., YAN Y.L., YUAN Z.P. Thermal performance study of organic flash cycle based on internal heat exchanger. J. Chem. Indus. **71** (07), 3080, **2020**.
22. LI J., GE Z., DUAN Y.Y., YANG Z. Design and performance analyses for a novel organic rankine cycle with supercritical subcritical heat absorption process coupling. Appl. Energ. **235**, 1400, **2019**.

23. GE Z., LI J., LIU Q., DUAN Y.Y., YANG Z. Thermodynamic analysis of dual-loop organic rankine cycle using zeotropic mixtures for internal combustion engine waste heat recovery. Energ. Convers. Manage. **166**, 201, **2018**.
24. XU W.C., DENG S., ZHAO L., ZHAO D.P., CHEN R.H. Identification of key affecting parameters of zeotropic working fluid on subcritical organic rankine cycle according limiting thermodynamic cycle. Energ. Convers. Manage. **197** (C), 111884, **2019**.
25. MENG J.H., WU H.C., WANG L., LU G., ZHANG K., YAN W.M.. Thermal management of a flexible controlled thermoelectric energy conversion-utilization system using a multi-objective optimization. Appl. Energ. **179**, 115721, **2020**.
26. LU X.Y., PAN Y.Y., XIE Y.L. Frost inhibition characteristics of superhydrophobic aluminum surface of micro-nano composite structure. Surf. Technol. **49** (3), 106, **2020**.
27. CHEN X.M., MA R.Y., ZHOU H.B., ZHOU X.F., CHE L.F., YAO S.H., WANG Z.K. Activating the microscale edge effect in a hierarchical surface for frosting suppression and defrosting promotion. Sci. Rep. **3** (1), 2507, **2013**.
28. WU X.M., CHU F.Q., CHEN Y.G. Theoretical analysis of droplets growth in early stage of frosting on hydrophobic surfaces. J. Chem. Indus. **66** (S1), 60, **2015**.
29. KIM S., KWANG, KIM J. Dropwise condensation modeling suitable for superhydrophobic surfaces. J. Heat Trans. **133** (8), 1, **2011**.
30. WU X.M., WANG W.C. Theoretical analysis of initial behavior of frost formed on a cold surface. J.Eng. Thermophys. **2**, 286, **2003**.
31. SU W., ZHANG X.S. Review of anti-frosting and defrosting methods on air source heat pump. J. Eng. Thermophys. **42** (09), 2195, **2021**.
32. YUAN X., DU Y.P., SU J. Approaches and potentials for pool boiling enhancement with superhigh heat flux on responsive smart surfaces: A critical review. Renew. Sust. Energ. Rev. **156**, 111974, **2022**.
33. LYN N., SHAO Z.B., HE H., WANG F., LIANG C.H., ZHANG X.S. Performance study of an active-passive combined anti-frosting method for fin-tube heat exchanger. Build. Environ. **222**, 109365, **2022**.